FAINT LUMINISCENT RING OVER THE SATURN'S POLAR HEXAGON.

Short title:
Brightness over the Saturn hexagon

Alberto Adriani[1,c], Maria Luisa Moriconi[2], Emiliano D'Aversa[1], Fabrizio Oliva[1] and Gianrico Filacchione[1]

[1] Institute of Space Astrophysics and Planetology of INAF, Via Fosso del Cavaliere 100, I-00133 Rome, Italy
[2] Institute of Atmospheric Sciences and Climate of CNR, Via Fosso del Cavaliere 100, I-00133 Rome, Italy
[C] corresponding author: alberto.adriani@iaps.inaf.it

Abstract

Springtime insolation is presently advancing across Saturn's North Polar Region. Early solar radiation scattered through the gaseous giant's atmosphere gives a unique opportunity to sound the atmospheric structure at its upper-troposphere/lower-stratosphere (UTLS) at high latitudes. Here we report the detection of a tenuous bright structure in Saturn's Northern polar cap in correspondence with the hexagon equator-ward boundary, observed by Cassini Visual and Infrared Mapping Spectrometer (VIMS) on June 2013. The structure is spectrally characterized by an anomalously enhanced intensity in the 3610-3730 nm wavelength range and near 2500 nm, pertaining to relatively low opacity windows between strong methane absorption bands.

Our first results suggest that a strong forward scattering by tropospheric clouds, higher in respect to the surrounding cloud deck, can be responsible for the enhanced intensity of the feature. This can be consistent with the atmospheric dynamics associated to the jet stream embedded in the polar hexagon.

Further investigations at higher spectral resolution are highly desirable to better assess the clouds vertical distribution and microphysics in this interesting region.

Keywords: planets and satellites: atmospheres - instrumentation: spectrographs - infrared: planetary systems - techniques: imaging spectroscopy - methods: data analysis - radiative transfer.

1. Introduction

Saturn's North Pole has been object of many studies and observations since the Voyager infrared images revealed for the first time its hexagonal-shaped vortex circulation (Godfrey et al., 1988). The Cassini mission added much more information about the atmospheric structure and composition (Baines et al. 2009; Sánchez-Lavega et al. 2014) since its arrival at Saturn. However, as the Saturn Orbit Insertion (SOI) of the Cassini spacecraft has occurred during the winter season on the Northern hemisphere, the first years of the mission have been suitable to study the northern regions of the atmosphere only through thermal emission at near- and mid-infrared wavelengths (Fletcher et al. 2008) or through fluorescence connected to the auroral emissions (Melin et al. 2011), whose contrast appears enhanced in low solar elevation conditions. In this paper we analyze a specific polar hexagon observation acquired by the VIMS infrared channel during a polar orbit hovering the grazing-illuminated polar cap moving from the night side towards the Sun.

2. Observations

A tenuous bright structure has been detected over Saturn's North Pole in June 25, 2013 by the Cassini's Visual and Infrared Mapping Spectrometer (VIMS, Brown et al. 2004), approximately coincident with the hexagon-shaped polar jet (Allison et al., 1990). The remarkably high 1s exposure time of this observation, though saturating a portion of the spectrum over the planet dayside, is particularly suitable for the detection of small spectral signatures. In particular the feature appears as an anomalously high signal around 2500 nm and in the 3600-3730 nm range. The latter is spectrally shaped as a double peak with maxima at 3665 and 3700 nm. Our very first hypothesis of a possible auroral emission had to be discarded due to its hexagonal shape, to the lack of the other spectral signatures typical of the H_3^+ emissions between 3 and 4 μm (Connerney and Satoh 2000) and to the amplitude of the signal at 2500 nm, that is two order of magnitude higher than the one expected by an auroral emission.

In Figure 1 (left panel) we show a RGB color composite image taken from the VIMS cube V1753141911 by selecting wavelengths corresponding to the 3665 and 3700 nm (doublet peaks) and thermal emission in the 5000 nm region, in order to enhance the shape of the bright structure. An idea of the latitudinal coverage and spatial resolution of the observation is given by the polar map projection of the same image shown in the right panel of Figure 1. The latitude values used in the map and hereafter in the text are calculated in the planetocentric coordinate system. The bright structure is latitudinally coincident with the equator-ward boundary of the hexagon, a region where the thermal emission from the deep atmosphere is strongly absorbed by optically thick tropospheric clouds.

The spatial average spectrum of the hexagonal bright structure is shown in Figure 2 for the 1700-3800 nm range, where our analysis is focused, together with the spectra averaged over the inner polar, the planetary limb (100-300 km above the 1-bar pressure level) and the night side regions. The radiance values in the plots are obtained from the raw data by using the radiometric calibration pipeline described in Filacchione et al. (2012). The shape of the doublet spectral feature is recognizable in all the spectra of the illuminated hemisphere of the planet, though very faint, but it is significantly more intense only over the hexagon. In Figure 2, each spectrum is color-coded according to the corresponding region as it appears from the associated image. In order to exclude that the bright structure belongs to an infrared auroral emission, Figure 2 also shows an infrared H_3^+ auroral emission spectrum for comparison, observed during a different orbit (cube V1595126852). Also this spectrum is a spatial average, calculated over the main auroral oval region. The comparison shows the absence of the many H_3^+ spectral signatures as well as the energy difference between the auroral emission and the bright structure. The spatial distribution of the auroral emission at 3530 nm (one of the most prominent H_3^+ emission lines) can be appreciated in the upper-left image (a) of Figure 2, while the image at the same wavelength in the observation under study (image (b) of Figure 2) shows the absence of any auroral signature.

The variation of the doublet's intensity with the illumination angle and the comparison with the limb spectrum (showing the 3.3 μm methane emission) suggest that the doublet is a true reflectance feature of the atmosphere. As shown in Figure 2 the doublet signature does not appear in the average spectrum taken on the planet's night side (black curve in Figure 2).

3. Data Analysis

A search for the existence of the doublet spectral feature has been carried out in several VIMS data, but a spectral doublet feature of such high intensity has only been found in recent observations of the equatorial zone and the Northern polar cap. The feature is located in a region of Saturn near-infrared spectrum where methane absorption is strong and its detection requires high exposure times to overcome the noise level. Furthermore, the anomalously high brightness is observable only at relatively high solar phase angles (128° for the observation here discussed). This indicates that the enhanced reflectivity could be ascribed to forward-scattering particles, probably comparable in sizes to the order of magnitude of the wavelength.

From the spectral point of view, the doublet is located between two very strong methane absorption bands at 3.3 and 3.8 μm and it represents a relatively weak transparency window of atmospheric transmission. The hexagonal shape of the structure suggests that it originates at tropospheric altitudes: in fact, the temperatures retrieved in Saturn polar regions from data by the Composite Infrared Spectrometer (CIRS) onboard Cassini (Fletcher et al. 2008, 2015), showed a circular stratospheric thermal field, not giving any hint of a possible hexagonal shape. Even stellar occultation data from VIMS at high latitude do not observe any 3700 nm doublet signature in the stratosphere (Kim et al. 2012).

In order to reproduce the observed spectra, we used a plane-parallel multiple-scattering line-by-line radiative transfer model (Oliva et al. 2013, 2014, 2015; Colosimo et al. 2010), based on the DISORT solver (Stamnes et al. 1988). We took into account only methane as absorbing gas, with molar fractions of different isotopes from Fletcher et al. (2007; 2009), absorption coefficients derived from the HITRAN 2012 database (Rothman et al. 2013), whereas the thermal profile is taken from Lindal et al. (1992). The cloud vertical structure consists of two particulate layers, one in the lower stratosphere and the other in the upper troposphere (see Table 1). The grain size distributions are assumed as log-normal for the stratospheric layer and as modified-gamma (Hansen, 1971) for the tropospheric one. Both layers are made of the grey component described in Karkoschka and Tomasko (2005). We limited our calculations to those ranges where the spectrum is unsaturated and not sensitive to gases other than methane. Thus, as shown in Figure 3, we exclude spectral ranges dominated by non-LTE emissions and absorptions by hydrogen, helium (collision induced absorption), phosphine, and ammonia.

As illustrated in Figure 3, we were able to fit spectra both in and out the observed structure by changing the vertical clouds structure. Synthetic spectra are mostly sensitive to the top pressure of the tropospheric cloud, its optical thickness and the stratospheric cloud optical thickness. We were not able to constrain the top pressure of the stratospheric cloud above 0.5 hPa and the base pressure of the tropospheric one below 700 hPa. Table 1 reports the best-fit values we obtained even if equally reliable fits can be achieved by changing the vertical extension of the clouds and adjusting the other parameters.

We would also point out that the methane correlated-k coefficients provided by Sromovsky et al. (2012) and the band model by Karkoschka & Tomasko (2010) were unable to reproduce the doublet methane feature, possibly leading to erroneous assignments of this spectral feature as due to molecules other than methane. We were able to fit the spectra only using a line-by-line approach referring to HITRAN 2012 database.

The transmission weighting functions of the atmosphere in clear sky conditions (Figure 4, left panel) give an indication of the atmospheric altitudes probed by the selected VIMS channels. As mentioned above the doublet's wavelengths and the 2500 nm wavelength are mostly sensitive to the properties of the tropospheric cloud, whereas the wavelengths around 1800, 2300 and 3500 nm are diagnostic of the lower stratosphere. This is consistent with the preliminary results we have obtained (Table 1) indicating that the variation of altitude of the tropospheric cloud is the key parameter to describe the observed feature. Hence the enhanced intensity of the doublet can be explained by the rising of the tropospheric cloud by about 5-10 km (15-30% of the scale height). The fact that the doublet appears weaker in other VIMS observations can be related to the different phase angles. In fact, in order to obtain the abovementioned fits at the high phase angle of the investigated observation, we had to use strong forward scattering cloud particles (Figure 4).

The region of the polar hexagon, where the high reflection feature is located, straddles the polar jet stream, whose wind velocities peak at about 76N, with a latitudinal variation of about 1.5° due to the non-axisymmetric nature of the hexagon (Baines et al. 2009). The bright feature is about 2° south of the jet and is very close in latitude to a maximum of the jet curvature (Sanchez-Lavega et al., 2014). Jet streams are usually associated to vertical motions and the rising air can easily produce condensation due to adiabatic cooling. Moreover the upwelling from lower altitudes can produce accumulation of particles and trace gases advected from deeper tropospheric layers at mid latitudes increasing the vertical mixing of gases. On the other hand, the rising air supplying the polar jet can introduce condensation nuclei in the upper troposphere and enhance local haze formation from local trace gases there present. Mixing with the air coming from below should be supported by the turbulence produced by the jet stream shear with the surrounding air. The formation of particles can increase the atmospheric optical thickness as well as the efficiency in blocking the thermal emission from below. Among the molecules candidates for condensation there are aldehydes - functional group H-C=O – and methanol that, even if never detected on Saturn, are predicted by some

chemical models (Moses et al., 2000) in Saturn's lower stratosphere and upper troposphere and eventually condensate if abundant enough.

5. Conclusions

We described an anomalously bright feature in Saturn's Northern polar hexagon, as recently observed by VIMS in high phase geometry. In particular, the brightness anomaly is observed at wavelengths around 3700 nm, where the methane absorption at VIMS resolution is shaped as a double peak. We were able to accurately reproduce the variation of Saturn's spectrum at the wavelengths of interest, showing their sensitivity to the atmospheric structure in the upper troposphere-lower stratosphere (UTLS). Simulations performed using either the methane correlated-k coefficients provided by Sromovsky et al. (2012) or the band model by Karkoschka & Tomasko (2010) failed in reproducing the doublet methane feature, thus we suggest to use HITRAN 2012 coefficients in this range. Our first results suggest that a strong forward scattering by a tropospheric cloud with a higher top in respect to the surrounding cloud deck can be responsible for the enhanced intensity of the feature. This can be consistent with the atmospheric dynamics associated to the jet stream embedded in the polar hexagon, being compatible with an increased abundance of particulates suggesting ongoing condensation and/or advection.

Further investigation of the doublet feature with higher spectral and spatial resolution will be necessary to more deeply assess the nature of the scattering particles. However this study, even at the present VIMS resolution, gives clues about the atmospheric structure of the UTLS region over Saturn's North Pole.

6. Acknowledgments

This work has been developed thanks to the financial support of the Italian Space Agency.

7. References

Baines K.H., T.W. Momary, L.N. Fletcher, et al. 2009, PSS, 57, 1671
Brown R.H., K. H. Baines, G. Bellucci, et al. 2004, Spa. Sci. Rev, 115, 111
Colosimo S.F., E. D'Aversa, A. Adriani, et al. 2010, EGU Congress, Vienna
Connerney J. E. P. and T. Satoh 2000, Phil. Trans. R. Soc. Lond. A, 358, 2471
Filacchione G., F. Capaccioni, M. Ciarniello, et al. 2012, Icarus, 220(2), 1064
Fletcher, L.N., P.G.J. Irwin, N.A. Teanby, et al. 2007, Icarus 188, 72.
Fletcher L.N., P. G.J. Irwin, G.S. Orton, et al. 2008, Science, 319, 79.
Fletcher L.N., G.S. Orton, N.A. Teanby, et al. 2009, Icarus, 199, 351.
Fletcher L.N., P.G.J. Irwin, J.A. Sinclair et al. 2015, Icarus, 250, 131.
Godfrey, D.A. 1988, Icarus 76, 335.
Hansen, J.E. 1971, JAS, 28, 1400.
Karkoschka, E. & Tomasko, M.G. 2005, Icarus, 179, 195
Karkoschka, E. & Tomasko, M.G. 2010, Icarus 205, 674
Kim, S.J., C.K. Sim, D.W. Lee, et al. 2012, PSS, 65(1), 122
Melin H., T. Stallard, S. Miller et al. 2011, GRL, 38, L15203
Lindal G.F. 1992, Astro.J., 103, 967
Moses J.I., E. Lellouch, B. Bezard, et al. 2000, Icarus 145, 166
Oliva F., A. Adriani, G.L. Liberti, et al. 2013, EPSC Abstracts Vol. 8, EPSC2013-158, European Planetary Science Congress 2013, London

Oliva F., A. Adriani, M.L. Moriconi, et al. 2014, 40th COSPAR Sci. Assembly, Moscow
Oliva F., A. Adriani, M.L. Moriconi, et al. 2015, Icarus, submitted
Rothman, L.S., I.E. Gordon, Y. Babikov, et al. 2013, JQSRT 130, 4
Sánchez-Lavega, A., T. del Río-Gaztelurrutia, R. Hueso, et al. 2014, GRL, 41, 1
Sromovsky, L.A., Fry, P. M.; Boudon, V. et al. 2012, Icarus 218, 1
Stamnes, K., S.C. Tsay, W. Wiscombe, et al., 1988, Applied Optics, 27, 2502.

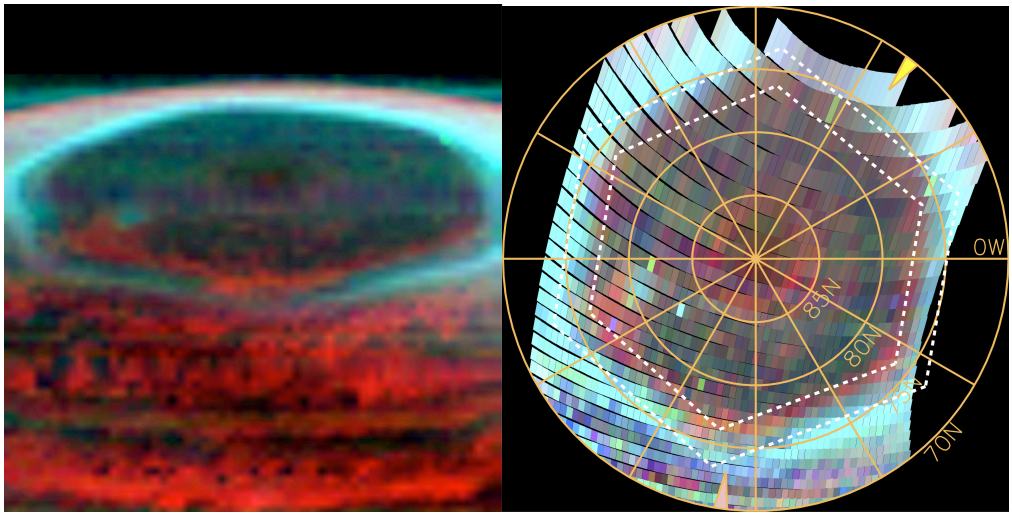

Figure 1. Left panel: an anomalously bright structure along the northern polar hexagon shown in a RGB color composite image. Red channel maps the intensity of thermal emission (taken at 4867 nm), whereas Green and Blue channels map the 3665 nm and 3700 nm wavelength respectively (doublet's peaks). Right panel: The same RGB image in a polar projection map, showing latitudinal coverage (planetocentric) and spatial resolution of the observation, as well as the position of the polar hexagon (dashed white lines) taken from Sanchez-Lavega et al. (2014). Arrows indicate the viewing (bottom, pink arrow) and illumination (top right, yellow arrow) directions.

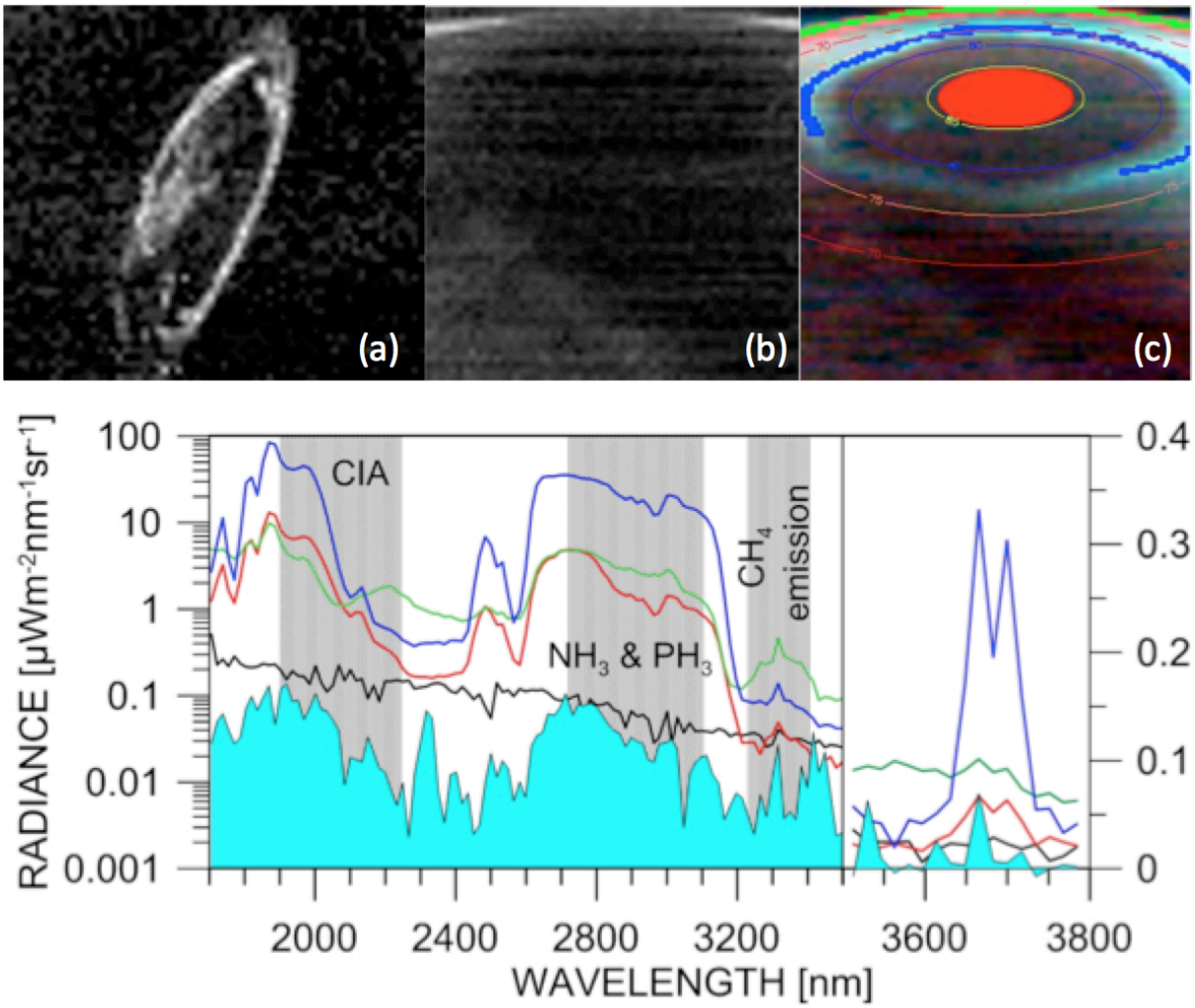

Figure 2.Spectral comparison in the polar region, from the same data cube shown in Figure 1. Bottom panel: the blue curve is an average spectrum over the bright hexagon feature, showing a very intense 3700 nm doublet; the green curve is a planetary limb average spectrum showing the typical 3300 nm methane emission complex; the red curve is an average spectrum taken over the central polar region; the black curve is an average spectrum from the dark side of the planet; the light blue shaded curve is a Saturn aurora spectrum (taken from the image shown on the upper left) shown for comparison of emission features. Refer to the top-right image to locate the actual averaging regions for the blue, red, and green spectra. Note the different axis scale used to enhance the 3700 nm doublet feature. Top: left(a) and middle(b) images are monochromatic at the same wavelength (3530 nm) from a cube showing a typical aurora (image (a)) and cube here under study. Top-right (c) image shows a RGB color composite similar to that of Figure 1 where the red thermal wavelength (4867 nm) has been replaced with the CH_4 Q branch at 3333 nm.

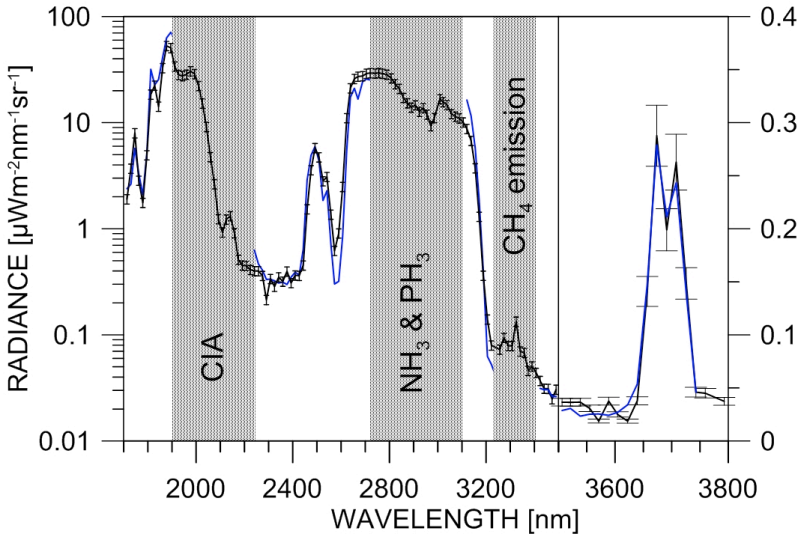

Figure 3. Best fitting result for a spectrum on the bright hexagon feature; measured radiance is shown in black, synthetic spectrum in blue; shaded in grey: spectral zones excluded from the simulations due to the presence of ammonia, phosphine, hydrogen collision induced absorption, and methane emission (see text); error bars account for an error of ±10% on the measured spectrum.

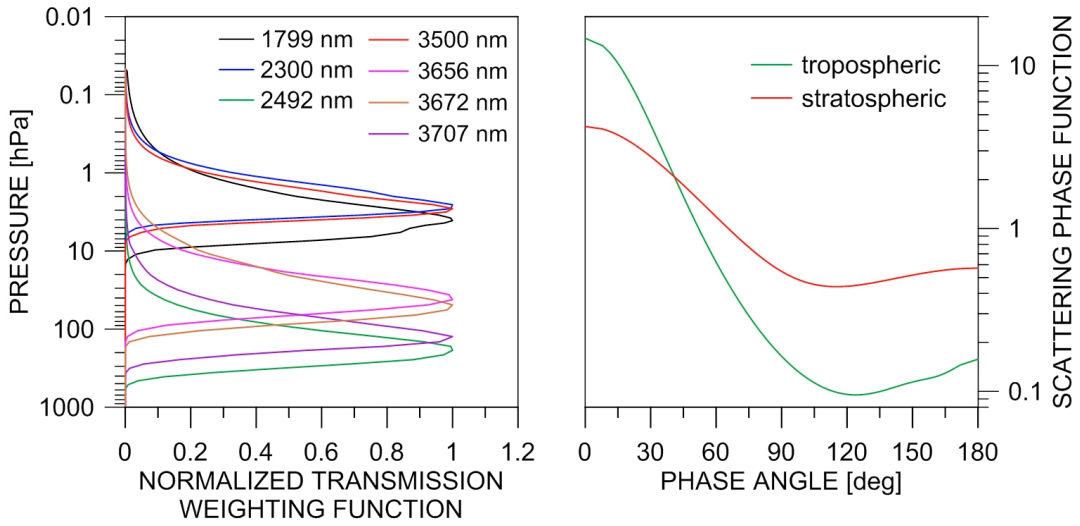

Figure 4: Left panel: Transmission weighting functions in clear sky computed from the atmospheric model described in the text. Right panel: single scattering phase functions at 3707 nm relative to the best fitting grain size distribution of the two cloud layers used in the model.

Table 1.

Cloud layers characteristics used in the best fitting simulation. r_{eff} and υ_{eff} are respectively the effective radius and variance of the particle size distribution.

		Off-bright feature (pixel 1-35)	On-bright feature (pixel 3-36)
	Incidence angle	**72.6°**	**72.4°**
	Emission angle	**58.8°**	**59.3°**
	Solar phase angle	**128.0°**	**128.0°**
Stratospheric Haze	Size Distribution	**Lognormal**	**Lognormal**
	r_{eff}, υ_{eff}	**0.25 µm, 0.2**	**0.25 µm, 0.2**
	Top Pressure	**< 0.5 hPa**	**< 0.5 hPa**
	Bottom Pressure	**114±11 hPa**	**95±9 hPa**
	Optical Depth	**0.006 @ 2 *µ*m**	**0.006 @ 2 *µ*m**
Tropospheric Haze	Size Distribution	**Gamma**	**Gamma**
	r_{eff}, υ_{eff}	**1.65 µm, 0.2**	**1.65 µm, 0.2**
	Top Pressure	**114±11 hPa**	**95±9 hPa**
	Bottom Pressure	**> 700 hPa**	**> 700 hPa**
	Optical Depth	**4.9 @ 2 *µ*m**	**4.9 @ 2 *µ*m**